

Determining Reactor Fuel Type from Continuous Antineutrino Monitoring

Patrick Jaffke* and Patrick Huber

Center for Neutrino Physics, Virginia Tech, Blacksburg 24061, Virginia, USA

(Received 20 January 2017; revised manuscript received 30 May 2017; published 8 September 2017)

We investigate the ability of an antineutrino detector to determine the fuel type of a reactor. A hypothetical 5-ton antineutrino detector is placed 25 m from the core and measures the spectral shape and rate of antineutrinos emitted by fission fragments in the core for a number of 90-d periods. Our results indicate that four major fuel types can be differentiated from the variation of fission fractions over the irradiation time with a true positive probability of detection at approximately 95%. In addition, we demonstrate that antineutrinos can identify the burnup at which weapons-grade mixed-oxide (MOX) fuel would be reduced to reactor-grade MOX, on average, providing assurance that plutonium-disposition goals are met. We also investigate removal scenarios where plutonium is purposefully diverted from a mixture of MOX and low-enriched uranium fuel. Finally, we discuss how our analysis is impacted by a spectral distortion around 6 MeV observed in the antineutrino spectrum measured from commercial power reactors.

DOI: 10.1103/PhysRevApplied.8.034005

I. INTRODUCTION

The end of the Cold War after the collapse of the Soviet Union in 1991 left the United States and Russia with a large number of surplus nuclear weapons [1]. Ultimately, the plutonium contained in these surplus nuclear weapons needs to be disposed of. There are various techniques proposed for the disposal of weapons plutonium (see, for instance, Ref. [2]), and one of these techniques is based on so-called mixed-oxide fuel (MOX), where a large part of the fissile content in regular reactor fuel is replaced with the to-be-disposed plutonium. This MOX fuel can be used in commercial light-water reactors and would thus allow one to convert some of the plutonium to usable energy. The remaining plutonium which is not fissioned will undergo a major change of its isotopic composition, rendering it less attractive for use in nuclear weapons. Moreover, whatever is left will be embedded in highly radioactive spent reactor fuel, making retrieval expensive and difficult. MOX fuel is successfully employed in Europe, particularly in France, where a significant number of power plants are using MOX fuel on an ongoing basis. In the MOX approach to plutonium disposal, the primary quantitative measure of reaching the disposition goal is given by burnup: fuel which has reached a certain burnup threshold will both have a significantly changed mix of plutonium isotopes and be sufficiently protected by its own radiation field. In this paper, we investigate how continuous antineutrino monitoring can be used as a complementary verification technique of both disposal goals by directly measuring the burnup and ratio of ^{239}Pu to ^{241}Pu , which serves as a proxy for the fraction of ^{240}Pu ; ^{240}Pu is not fissile and thus

does not have its own direct antineutrino signature. In addition, we study the hypothetical scenario of the intentional removal of plutonium.

The monitoring of nuclear reactors via antineutrino emission was first postulated nearly 40 years ago by Borovoi and Mikaelyan [3]. This concept has seen a recent resurgence as a safeguard or verification technique [4–9], where antineutrinos offer the unique advantages of independence of operation declarations and the ability to recover from a loss of continuity [10]. This type of reactor monitoring would require surface-level detector technology, which has yet to be demonstrated with sufficient fidelity but is the current goal of many short-baseline neutrino experiments [11].

Antineutrino monitoring relies on the fact that fissions of different fissile nuclides, such as $^{235,238}\text{U}$ or $^{239,241}\text{Pu}$, produce different spectral shapes in antineutrino energy. As the antineutrino yields for each main fissile are sufficiently different, one can separate a total reactor antineutrino signal into its fissile components and infer the fission rates. Thus, an overall measurement of the rate of antineutrinos will determine the power of the reactor, while a spectral decomposition can infer the core content. These techniques were employed previously [6,10] to study the capabilities of antineutrinos based on real-world scenarios. We use a similar process in this work.

II. ANALYSIS PROCEDURE

The fuel evolution of the reactor of interest is simulated, and, thus, we obtain the fission rates throughout the irradiation cycle. This allows one to compute the total antineutrino spectrum by weighting these fission rates with the appropriate antineutrino yields from a single fission of each fissioning isotope. The uncertainties in these yields

*Corresponding author.
pjaffke@vt.edu

can be reduced with a previous calibration of the antineutrino detector to a core with known composition. This calibration would be performed by matching the measured spectra at the test reactor to a reference spectrum at various steps of the fuel evolution. Residual differences would become calibration constants of the detector and this procedure could be performed with multiple reactors to ensure that the constants are reactor independent. Recently, the Daya Bay Collaboration reported such a reference spectrum [12], which clearly demonstrated a change in antineutrino spectrum with burnup. Here, we assume this calibration has been performed. The total antineutrino signal represents the “observed” spectrum in our simulated cases. The expected events are separated into energy bins to acquire the spectral shape, which is represented by

$$n_i = N \int_{E_i - \Delta E/2}^{E_i + \Delta E/2} \sigma(E) \vec{\mathcal{F}} \cdot \vec{S}(E) dE, \quad (1)$$

with the width of the energy bin ΔE , the interaction cross section $\sigma(E)$ [13], the fission-rate vector $\vec{\mathcal{F}}$, where $\vec{\mathcal{F}} = [\mathcal{F}_{\text{U235}}, \mathcal{F}_{\text{U238}}, \mathcal{F}_{\text{Pu239}}, \mathcal{F}_{\text{Pu241}}]$, and the vector of anti-neutrino yields from each fissile $\vec{S}(E)$. We take the Huber-Mueller [14,15] $\vec{S}(E)$, which are converted from the measurements of Schreckenbach [16,17], except for ^{238}U . The normalization N takes into account the detector size, location, and overall efficiency. We assume a baseline short enough to avoid neutrino oscillations via active neutrinos. The choice of ΔE must be small enough to allow for good resolution in the spectral shape. We have chosen $\Delta E = 250$ keV and a detection threshold of 2 MeV. Large-scale experiments have demonstrated subpercent energy calibration [18–20], but previous studies [11] have shown that an event-by-event energy resolution on the order of $15\%/\sqrt{E}(\text{MeV}^{-1/2})$ is sufficient for this type of analysis and that energy-scale uncertainties on the order of 1% to 2% have a negligible impact. Future short-baseline detectors are aiming to match or exceed this precision; see for instance, Ref. [21].

One can compute a log-likelihood ratio by comparing the observed spectrum, created by weighting the reactor-simulated fission-rate vector $\vec{\mathcal{F}}_S$ with the yields $\vec{S}(E)$, to the expected spectral shape of Eq. (1). Minimizing the resulting χ^2 function, given as

$$\chi^2(\vec{\mathcal{F}}) = \sum_i^N \frac{[n_i(\vec{\mathcal{F}}) - n_i']^2}{n_i'}, \quad (2)$$

provides the best-fit fission-rate vector $\vec{\mathcal{F}}$ (or maximum-likelihood estimate), where the observed events from $\vec{\mathcal{F}}_S$ in bin i are represented as n_i' . This measurement of the fission-rate vector is then used to determine the core type and progression along its irradiation cycle. Detection statistics

are simulated by randomizing the n_i' 's with a Poisson distribution. We assume that detection statistics dominate the error budget as precise detector calibration and simulation have been achieved below the few-percent level and accurate background measurements have been incorporated into previous calibration techniques [22].

The simulated reactor is a Westinghouse-style light-water reactor (LWR) loaded with various core compositions. The details of the reactor simulation and the core configuration and characteristics are given in Ref. [23]. Our analysis is primarily concerned with four core types. The first is weapons-grade MOX (WGMOX) used in the LWR, corresponding to the actual disposition case. The second is reactor-grade MOX (RGMOX), which corresponds to the plutonium vector of discharged uranium-based fuel and usually is part of a fuel cycle which includes reprocessing of spent fuel. The third fuel type is a mixture of two-thirds low-enriched uranium (LEU) fuel and one third of WGMOX. One third corresponds approximately to the MOX fraction used in France, but this is obviously RGMOX. Finally, the fourth core is a full LEU core. All four cores are simulated to run for a total of 500 d of irradiation at full power, corresponding to a burnup of 21-MW d/kg heavy metal. The fission rates from our simulated cases will have an implicit time dependence $\vec{\mathcal{F}}(t)$ as the fuel changes composition during irradiation. Thus, Eq. (1) is modified with an integration over the detection time T , which implies that the observed spectral shape will depend on *when* the detector monitors the reactor.

III. SIMULATION RESULTS

We simulate 200 sample cases for each of the four core types and four different detection periods. Each individual case represents a different Poisson-randomized antineutrino spectrum via Eq. (1) with the $\vec{\mathcal{F}}_S$ from the reactor simulation. We assume a detector mass of 5 ton at 25 m from the reactor core with 90-d observation periods. Each case is minimized via Eq. (2), producing a best-fit core-averaged $\vec{\mathcal{F}}$ for that detection period and fuel content. In Fig. 1, we plot the total plutonium fission fraction, $(\mathcal{F}_{\text{Pu239}} + \mathcal{F}_{\text{Pu241}})/|\vec{\mathcal{F}}|$, versus the ^{239}Pu fission fraction $\mathcal{F}_{\text{Pu239}}/|\vec{\mathcal{F}}|$ for each of the 200 sample cases over the four core types (colors) and four detection periods (symbols). The open circles, squares, triangles, and diamonds indicate the starting day of the measurement τ_0 ; thus, open circles mean that the reactor is monitored from the start of irradiation for 90 consecutive days. The large black circles indicate the average fission fractions over all 200 cases, and the black crosses are the average fission fractions calculated with $\vec{\mathcal{F}}_S$.

We can see that for the first 90-d measurement (the circles), the cores appear as expected. The pure LEU core (blue) contains a majority of uranium fissions and very little plutonium. The core with one-third WGMOX (red)

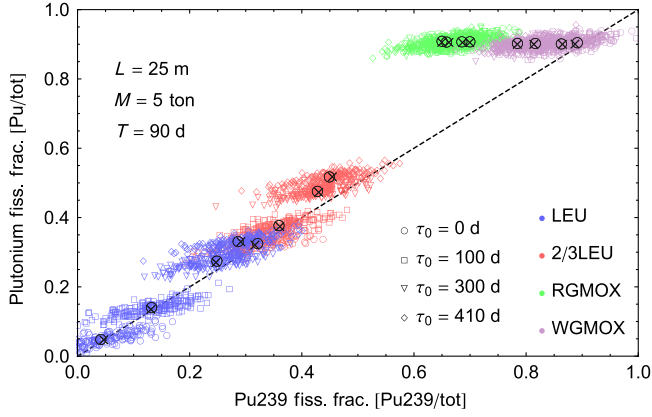


FIG. 1. Plot of the $\bar{\nu}$ -derived best-fit total plutonium versus ^{239}Pu fission fractions of 200 cases each for all four different fuel inventories (colors) and over four different detection start dates τ_0 (symbols). The progression of fuel is illustrated by the movement of the centroids (the black markers) for each set. Circular centroids are $\bar{\nu}$ derived and the crosses are directly from the simulated fission rates. The dashed line is the physically real plutonium boundary. We assume a 5-ton detector at a 25-m baseline over 90-d periods.

contains a sizable amount of plutonium initially and the plutonium is a high-percentage ^{239}Pu , as the centroid falls near the pure ^{239}Pu dashed line. For the MOX cores, the reactor-grade plutonium (green) begins far from the purity line and has mostly plutonium fissions. The WGMOX core (purple) begins on the purity line and also has a majority of plutonium fissions. We also note that the average fission fractions derived from this antineutrino analysis are within a few percent of the values directly from the reactor simulations.

From Fig. 1, we note that the initial state of the mixed LEU + WGMOX core (the red circles) looks nearly identical to that of the last detection period of the pure LEU core (the blue diamonds). This degeneracy can be broken when we consider continuous antineutrino monitoring. With continuous monitoring, one would know the starting irradiation time and relative power from the rate measurement. With multiple measurements of the antineutrino spectrum, one could infer a core inventory based on the trajectory of two consecutive measurements, say, $\tau_0 = 0$ d and $\tau_0 = 100$ d. A trajectory that moves along the pure ^{239}Pu dashed line is composed mostly of LEU. Horizontal shifts are cores that contain mostly MOX.

To acquire information on the plutonium grade, an important factor in weapons production [24], one can use a ratio of the plutonium fission rates. We use the ratio of ^{239}Pu fission rate to the total plutonium fission rate, which we label as the plutonium fission grade (G_{Pu}). We use $G_{\text{Pu}} = 90\%$ as the disposition goal, as the thermal fission cross section of ^{241}Pu is 35% higher than the one of ^{239}Pu . Thus, in a mixture of 93% ^{239}Pu and 7% ^{241}Pu , 90% of all fission will take place in ^{239}Pu . We find, based on this

TABLE I. Differential-burnup analysis (DBA) of the ^{239}Pu fission fraction $\Delta F_{\text{Pu}239}$ and the plutonium fission fraction ΔF_{Pu} between the initial $\tau_0 = 0$ d measurement period and the three following measurement periods in percent. The DBA is conducted for the four simulated cores and is given as ordered pairs. Also listed are the DBA results for the removal cases where no fresh WGMOX assemblies (nominal), 8, or all 20 are replaced with LEU fuel.

Differential burnup $\Delta \vec{F} = [\Delta F_{\text{Pu}239}, \Delta F_{\text{Pu}}]$ in percent			
	$\tau_0 = 100$ d	$\tau_0 = 300$ d	$\tau_0 = 410$ d
LEU	[218, 201]	[498, 493]	[589, 616]
2/3 LEU	[11.8, 16.1]	[33.2, 46.6]	[39.9, 59.5]
RGMOX	[-2.05, -0.01]	[-5.96, -0.10]	[-7.10, 0.17]
WGMOX	[-3.20, -0.39]	[-8.41, -0.25]	[-12.0, -0.23]
Nominal	[8.40, 14.0]	[30.0, 38.0]	[31.1, 48.9]
8 removed	[10.1, 14.6]	[30.3, 40.9]	[40.9, 54.2]
20 removed	[20.5, 20.5]	[44.9, 52.1]	[57.4, 68.2]

antineutrino measurement, that 16% (31%) of the WGMOX (LEU + WGMOX) cores remain above this goal at the final [(410–500)-d] measurement period. The sensitivity to downgrading the plutonium is worse in the mixed core, as the uranium absorbs some of the total fission rate, thus slowing the progression of plutonium fissions from weapons grade to reactor grade. In addition, this measurement represents a core-averaged plutonium ratio, so a lower G_{Pu} requirement would be necessary to ensure that all assemblies fall below the weapons barrier; otherwise, an assembly-by-assembly technique would need to be employed as well [25].

The trajectory and the absolute distance traveled in the fission-fraction plane can be calculated from Fig. 1 and compared between different cores and different measurement periods. For example, the LEU cores both burn along the same trajectory, but the pure LEU core has a much larger difference between two adjacent measurement periods than the mixed core. This quantity, which we label the differential burnup, is given by

$$\Delta \vec{F} = \frac{\vec{F}(t_f) - \vec{F}(t_i)}{|\vec{F}(t_f)|}, \quad (3)$$

where the fission fraction $\vec{F}(t)$ is created from the best-fit values of the fission-rate vector $\vec{\mathcal{F}}(t)$. Thus, Eq. (3) represents the percent change along a particular fission-fraction trajectory. The differential burnup in the ^{239}Pu trajectory $F_{\text{Pu}239} = \mathcal{F}_{\text{Pu}239}/|\vec{\mathcal{F}}|$ and the total plutonium trajectory $F_{\text{Pu}} = (\mathcal{F}_{\text{Pu}239} + \mathcal{F}_{\text{Pu}241})/|\vec{\mathcal{F}}|$ between the four measurement periods and the four simulated cores are shown in Table I.

We note that both LEU-type cores have a positive ΔF_{Pu} across all time steps, indicating that these cores are producing plutonium. However, the LEU core mixed with

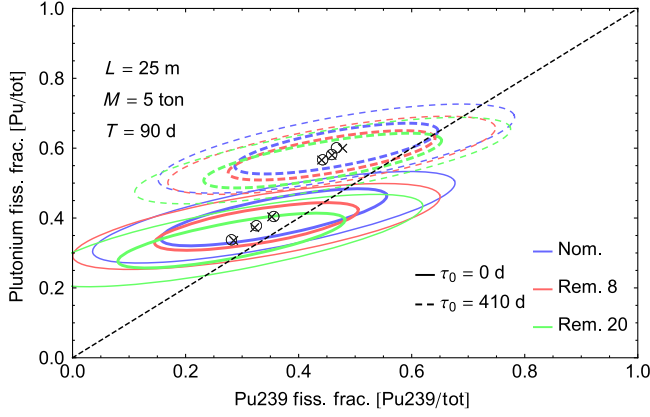


FIG. 2. Plot of the allowed region contours of the best-fit ^{239}Pu and total plutonium fission fractions at the first and last measurement periods for three removal scenarios. The contours are derived by fitting Gaussian ellipses to the scatter of the 200 cases. The thick inner ellipse denotes the 1σ quartile, and the thin outer ellipse the 2σ quartile. Circular centroids are $\bar{\nu}$ derived and crosses are directly from the simulated fission rates. The dashed line is the physically real plutonium boundary. We assume a 5-ton detector at a 25-m baseline over 90-d periods.

WG plutonium has a significantly smaller ΔF_{Pu} , indicating that the *rate* of plutonium production in the mixed core is dramatically slower by about an order of magnitude for all time steps. In addition, the grade of the plutonium, related to $\Delta F_{\text{Pu}239}$, decreases faster for the WGMOX core than the RGMOX core. This difference is much more subtle and develops slowly, but results in an almost doubling of $\Delta F_{\text{Pu}239}$, as can be seen in Table I.

Another possible scenario is the intentional removal of plutonium from a core, such as the mixed LEU and WGMOX core [23]. The mixed core uses a total of 48 MOX assemblies, 28 of which are once or twice irradiated and are therefore not considered WGMOX any longer. This staggered burning is used in reactor operation to flatten the neutron flux profile. We investigate three scenarios. The first is the nominal run with no removal of the fresh WGMOX assemblies. The second considers removing eight fresh WGMOX assemblies from the periphery of the reactor and replacing them with LEU assemblies. The fission rate at the edge of the reactor core is relatively low, and thus this case will be a particular challenge for antineutrino monitoring. The final case is a full removal and replacement of all (20) fresh WGMOX assemblies. Figure 2 shows the exclusion contours of these scenarios in the $F_{\text{Pu}239}-F_{\text{Pu}}$ plane at the initial and final time step.

For the removal cases, we see that the differential-burnup vectors are all aligned in relatively the same direction, and the magnitudes are only slightly different. The differences between the removal cases are much less pronounced than those for the full cores, as seen in Table I, and there is a significant amount of overlap between the contours. It is also apparent that the equilibrium fission rates for each

removal scenario are nearly identical, making any differences in the resulting $\bar{\nu}$ signal more difficult to detect at later irradiation times.

The analyses in Figs. 1 and 2 and Table I demonstrate the process by which an antineutrino detector would infer the core content of a nuclear reactor. Several time steps are needed to determine the progression of the fuel and identify the differential burnup. The sign and magnitude resulting from DBA can distinguish between LEU, mixed LEU + MOX, and MOX cores easily, but the difference between RGMOX and WGMOX is more subtle. An absolute measurement of the fission fractions can help to distinguish the latter cases. Next, we present the sensitivity analysis for these absolute measurements.

IV. SENSITIVITY STUDIES

We proceed to determine the true and false-positive rates (FPRs) from the data generated so far. First, the simulated cases are binned along an axis; Fig. 3 provides the projection of Fig. 1 onto its x axis of ^{239}Pu fission fraction in 2.5%-wide bins. We fit the resulting histograms with a normal distribution, determining the mean and standard deviation. The resulting normal distributions are used to compute the true and false positive rates of determining the core composition for a given time period. To allow a simple summary, we choose the critical value in this variable such that the false-negative and false-positive rates are equal, and we will quote this common value. In the language of a receiver-operating characteristic, this value corresponds to the balance point.

One can determine the false-positive rate and the balance point for the four core and measurement-period histograms using different fission fractions. As one would expect from Fig. 3, we observe a very small FPR (i.e., there is very little

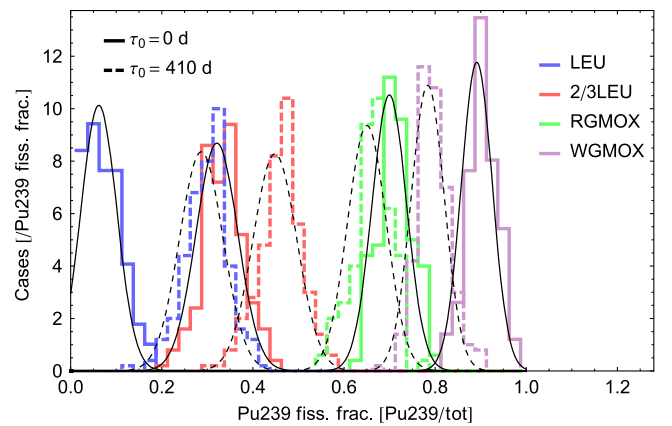


FIG. 3. Histogram of the $\bar{\nu}$ -determined ^{239}Pu fission fraction of the simulated cases for the first (solid curves) and last (dashed curves) measurement times and four core compositions, and the corresponding fitted Gaussian distributions (the thin curves). This plot represents Fig. 1 projected onto its x axis in 2.5%-wide bins. We assume a 5-ton detector at a 25-m baseline over 90-d periods.

TABLE II. Upper triangular portion of the core-identification FPR matrices using the ^{239}Pu fission fraction. Each upper triangular cell corresponds to the percentage of falsely identified cores between the various core compositions. This is done for three considered locations of the spectral structure (no bump, a ^{235}U bump, and a ^{239}Pu bump) and for the first ($\tau_0 = 0$ d) and last ($\tau_0 = 410$ d) measurement periods. The total FPR matrix is symmetric, as expected. The FPR between the RGMOX and WGMOX cores is reduced by about a factor of 3 when using the plutonium grade as a diagnostic.

		False-positive rates								
		No bump			^{235}U bump			^{239}Pu bump		
		LEU+MOX	RGMOX	WGMOX	LEU+MOX	RGMOX	WGMOX	LEU+MOX	RGMOX	WGMOX
First	LEU	0.119%	$<10^{-4}\%$	$<10^{-4}\%$	0.00380%	$<10^{-4}\%$	$<10^{-4}\%$	$<10^{-4}\%$	$<10^{-4}\%$	$<10^{-4}\%$
	LEU+MOX		$<10^{-4}\%$	$<10^{-4}\%$		$<10^{-4}\%$	$<10^{-4}\%$		$<10^{-4}\%$	$<10^{-4}\%$
	RGMOX			0.377%			0.0318%			$<10^{-4}\%$
Last	LEU	4.60%	0.00290%	$<10^{-4}\%$	0.612%	$<10^{-4}\%$	$<10^{-4}\%$	$<10^{-4}\%$	$<10^{-4}\%$	$<10^{-4}\%$
	LEU+MOX		1.31%	0.00385%		0.0533%	$<10^{-4}\%$		$<10^{-4}\%$	$<10^{-4}\%$
	RGMOX			4.61%			1.21%			$<10^{-4}\%$

overlap between the fitted Gaussians) during the first measurement period (approximately 0.1% between the LEU cores and about 0.4% between the MOX cores). The second measurement shows a more significant FPR of approximately 1% between both of the LEU cores and both of the MOX cores. The third measurement begins to show a higher FPR between the RGMOX and mixed LEU + WGMOX cores, but only around 0.3%. The FPR between the LEU cores is approximately 3%, and that between the MOX cores is about 1.8%. The last measurement shows a FPR between the LEU cores at 4.6%, between the MOX cores at 4.6%, and between the LEU + WGMOX and RGMOX cores at approximately 1.3%. The information for the first and last measurements is given quantitatively in Table II. One can see that the FPR grows with a larger burnup, indicating that the core compositions become more similar as they approach equilibrium.

The low FPR indicate that only about 5% of the cases will result in a misidentification of the core type. Multiple tests with different $\vec{F}(t)$ values can isolate and enhance this accuracy. For example, using the plutonium or uranium fission fraction provides very good separation between the LEU and pure MOX cores, but it is completely impossible to distinguish between RGMOX and WGMOX. Using the ^{239}Pu grade, the FPR drops by about a factor of 3 between the RGMOX and WGMOX cores, but it increases drastically for the LEU cores due to the lower plutonium fission fractions. For the removal scenarios, the FPRs are consistently above 50% among all measurements, scenarios, and fission-fraction diagnostics, implying that differentiation among them is beyond the capabilities of antineutrino monitoring. This is primarily because antineutrinos measure core-averaged quantities instead of individual assemblies.

Recently, a spectral distortion was observed near 5 MeV (positron energy) in the reactor antineutrino flux of multiple large-statistics experiments [18–20]. The origin of this so-called bump is unknown, but several theories

have been explored [26–28]. Irrespective of the bump explanation, one can examine the impact of the spectral feature on the fuel determination by artificially placing the observed bump in the converted antineutrino yields.

We choose to place the spectral feature in either ^{235}U or ^{239}Pu . Using Fig. 2 in Ref. [18], the bump is modeled as a Gaussian distribution added to the original $\vec{S}(E)$ value, where the mean and the variance are determined by a least-squares fit. We note that the normalization of the Gaussian is fixed by the fission fractions and the overall neutrino rate in the relevant energy bins. The three Gaussian best-fit parameters vary by only a small amount when fixing them instead by Ref. [19] or Ref. [20]. With these new artificial yields, we repeat the process outlined above and generate more sample cases. As expected, a new spectral distortion in either ^{235}U or ^{239}Pu enhances the abilities of an antineutrino detector to distinguish between fuel types. A bump in ^{235}U has the effect of pinching the spread of F_{Pu} in Fig. 1, as the ^{235}U fission rate, now easily identified by the spectral distortion, essentially fixes the total plutonium fissions. A bump in ^{239}Pu pinches the distributions along the axis in the $F_{\text{Pu}239} - F_{\text{Pu}}$ plane, according to the core content. This pinching also has the effect of reducing the variance in the Gaussian distributions found in Fig. 3, which lowers the FPR. Overall, Table II shows that this procedure reduces the FPR by at least a factor of 3 if the ^{235}U spectrum contains the bump, and below $10^{-4}\%$ for a ^{239}Pu bump. The FPRs remain at or above about 50% for all removal scenarios across all measurement periods. The sensitivity to downgrading is also enhanced by the bump location. Less than 1% (20%) of the WGMOX (LEU + WGMOX) cores return $G_{\text{Pu}} > 90\%$ at the last measurement period with a ^{239}Pu bump.

V. CONCLUSION

This work explores the abilities of a surface-deployed antineutrino detector to determine the core composition of

the reactor it is monitoring via continuous spectral measurements. The spectrum, with an interaction threshold of 2 MeV and binned into 250-keV bins, is fitted to an event distribution providing best-fit values for the fission rates of $^{235,238}\text{U}$ and $^{239,241}\text{Pu}$. These best-fit fission rates are combined into various fractions and we determine that, for 500 d of irradiation in a LWR, which will downgrade a full WGMOX core to RGMOX, we can establish this average downgrade with 84% confidence based on antineutrino monitoring. For a one-third WGMOX and two-thirds LEU core, we can determine the average downgrade with 69% confidence. Multiple measurement periods of 90 d within the irradiation cycle can differentiate between our four major core compositions with 95% accuracy. This is done mostly by comparing it to the ^{239}Pu fission fraction, but it can be reinforced with other fission fractions as well. Detecting the removal of plutonium from a mixed LEU and WGMOX core with an antineutrino detector is found to be incredibly difficult and highly reliant on the first measurement period. The existence of a spectral distortion in either the ^{235}U or ^{239}Pu antineutrino yields only enhances the monitoring capabilities mentioned above, except for the detection of an intentional removal of plutonium.

ACKNOWLEDGMENTS

We would like to acknowledge A. Bernstein, N. Bowden, and A. Erickson for the useful discussions and their comments on an earlier version of this manuscript. This work was supported by the U.S. Department of Energy National Nuclear Security Administration under Award No. DE-AC52-07NA27344 via Subaward No. B612358 from Lawrence Livermore National Laboratory.

[1] National Academy of Sciences, *Management and Disposition of Excess Weapons Plutonium* (National Academies Press, Washington, DC, 1994).

[2] Frank von Hippel and Gordon MacKerron, International Panel on Fissile Materials Report No. 13, 2015.

[3] A. A. Borovoi and L. A. Mikaelyan, Possibilities of the practical use of neutrinos, *Sov. At. Energy* **44**, 589 (1978).

[4] Adam Bernstein, Yi-fang Wang, Giorgio Gratta, and Todd West, Nuclear reactor safeguards and monitoring with antineutrino detectors, *J. Appl. Phys.* **91**, 4672 (2002).

[5] A. Bernstein, N. S. Bowden, A. Misner, and T. Palmer, Monitoring the thermal power of nuclear reactors with a prototype cubic meter antineutrino detector, *J. Appl. Phys.* **103**, 074905 (2008).

[6] Eric Christensen, Patrick Huber, and Patrick Jaffke, Antineutrino reactor safeguards—A case study, *Sci. Global Secur.* **23**, 20 (2015).

[7] K. M. Heeger, M. N. Tobin, B. R. Littlejohn, and H. P. Mumm, Experimental parameters for a reactor antineutrino experiment at very short baselines, *Phys. Rev. D* **87**, 073008 (2013).

[8] S. Oguri, Y. Kuroda, Y. Kato, R. Nakata, Y. Inoue, C. Ito, and M. Minowa, Reactor antineutrino monitoring with a plastic scintillator array as a new safeguards method, *Nucl. Instrum. Methods Phys. Res., Sect. A* **757**, 33 (2014).

[9] G. Boireau *et al.* (NUCIFER Collaboration), Online monitoring of the Osiris reactor with the Nucifer neutrino detector, *Phys. Rev. D* **93**, 112006 (2016).

[10] Eric Christensen, Patrick Huber, Patrick Jaffke, and Thomas E. Shea, Antineutrino Monitoring for Heavy Water Reactors, *Phys. Rev. Lett.* **113**, 042503 (2014).

[11] N. S. Bowden, K. M. Heeger, P. Huber, C. Mariani, and R. B. Vogelaar, Applied Antineutrino Physics 2015—Conference summary, [arXiv:1602.04759](https://arxiv.org/abs/1602.04759).

[12] F. P. An *et al.* (Daya Bay Collaboration), Evolution of the Reactor Antineutrino Flux and Spectrum at Daya Bay, *Phys. Rev. Lett.* **118**, 251801 (2017).

[13] P. Vogel and John F. Beacom, Angular distribution of neutron inverse beta decay, $\bar{\nu}_e + p \rightarrow e^+ + n$, *Phys. Rev. D* **60**, 053003 (1999).

[14] Patrick Huber, Determination of antineutrino spectra from nuclear reactors, *Phys. Rev. C* **84**, 024617 (2011).

[15] Th. A. Mueller *et al.*, Improved predictions of reactor antineutrino spectra, *Phys. Rev. C* **83**, 054615 (2011).

[16] K. Schreckenbach, G. Colvin, W. Gelletly, and F. Von Feilitzsch, Determination of the antineutrino spectrum from ^{235}U thermal neutron fission products up to 9.5 MeV, *Phys. Lett.* **160B**, 325 (1985).

[17] A. A. Hahn, K. Schreckenbach, G. Colvin, B. Krusche, W. Gelletly, and F. von Feilitzsch, Antineutrino spectra from ^{241}Pu and ^{239}Pu thermal neutron fission products, *Phys. Lett. B* **218**, 365 (1989).

[18] Feng Peng An *et al.* (Daya Bay Collaboration), Measurement of the Reactor Antineutrino Flux and Spectrum at Daya Bay, *Phys. Rev. Lett.* **116**, 061801 (2016).

[19] J. H. Choi *et al.* (RENO Collaboration), Observation of Energy and Baseline Dependent Reactor Antineutrino Disappearance in the RENO Experiment, *Phys. Rev. Lett.* **116**, 211801 (2016).

[20] J. I. Crespo-Anadón (for the Double Chooz Collaboration), in *Proceedings of the Neutrino Oscillation Workshop (NOW 2014), Otranto, Italy, 2014*, edited by P. Bernardini, G. Fogli, and E. Lisi, [*Nucl. Phys. B, Proc. Suppl.* 265–266, 99 (2015)].

[21] J. Ashenfelter *et al.* (PROSPECT Collaboration), The PROSPECT physics program, *J. Phys. G* **43**, 113001 (2016).

[22] F. P. An *et al.* (Daya Bay Collaboration), Measurement of electron antineutrino oscillation based on 1230 days of operation of the Daya Bay experiment, *Phys. Rev. D* **95**, 072006 (2017).

[23] Anna Erickson, Adam Bernstein, and Nathaniel Bowden, Reactors as a source of antineutrinos: The effect of fuel loading and burnup for mixed oxide fuels, [arXiv:1612.00540](https://arxiv.org/abs/1612.00540).

[24] J. Carlson, J. Bardsley, V. Bragin, and J. Hill, in *Proceedings of the IAEA Symposium on International Safeguards, Vienna, 1997* (International Atomic Energy Agency, Vienna, 1999), pp. 110–111.

[25] Naeem M. Abdurrahman, Robert C. Block, Donald R. Harris, Rudolf E. Slovacek, Yong-Doek Lee, and

- Francisco Rodriguez-Vera, Spent-fuel assay performance and Monte Carlo analysis of the Rensselaer slowing-down-time spectrometer, *Nucl. Sci. Eng.* **115**, 279 (1993).
- [26] A. C. Hayes, J. L. Friar, G. T. Garvey, Duligur Ibeling, Gerard Jungman, T. Kawano, and Robert W. Mills, Possible origins and implications of the shoulder in reactor neutrino spectra, *Phys. Rev. D* **92**, 033015 (2015).
- [27] Patrick Huber, Reactor antineutrino fluxes—Status and challenges, *Nucl. Phys.* **B908**, 268 (2016).
- [28] A. C. Hayes and Petr Vogel, Reactor neutrino spectra, *Ann. Rev. Nucl. Part. Sci.* **66**, 219 (2016).